BJP British Journal of Pharmacology

DOI:10.1111/bph.12216
www.brjpharmacol.org

RESEARCH PAPER

YL529, a novel, orally available multikinase inhibitor, potently inhibits angiogenesis and tumour growth in preclinical models

Youzhi Xu*, Hongjun Lin*, Nana Meng*, Wenjie Lu, Guobo Li, Yuanyuan Han, Xiaoyun Dai, Yong Xia, Xiangrong Song, Shengyong Yang, Yuquan Wei, Luoting Yu and Yinglan Zhao

State Key Laboratory of Biotherapy and Cancer Center, West China Hospital, West China Medical School, Sichuan University, Chengdu, China

Correspondence
Ying-Lan Zhao and Luo-ting Yu, State Key Laboratory of Biotherapy and Cancer Center, West China Hospital, West China Medical School, Sichuan University, 17#, 3rd Section, Ren min South Road, Chengdu 610041, China. E-mail: alancenxb@sina.com

*These authors contributed equally to this work.

Keywords
YL529; small molecular multikinase inhibitor; anti-angiogenesis; anti-proliferation

Received
9 April 2012
Revised
1 February 2013
Accepted
20 March 2013

BACKGROUND AND PURPOSE
Targeted chemotherapy using small-molecule inhibitors of angiogenesis and proliferation is a promising strategy for cancer therapy.

EXPERIMENTAL APPROACH
YL529 was developed via computer-aided drug design, *de novo* synthesis and high-throughput screening. The biochemical, pharmacodynamic and toxicological profiles of YL529 were investigated using kinase and cell viability assays, a mouse tumour cell-containing alginate bead model, a zebrafish angiogenesis model and several human tumour xenograft models in athymic mice.

KEY RESULTS
In vitro, YL529 selectively inhibited the activities of VEGFR2/VEGFR3 and serine/threonine kinase RAF kinase. YL529 inhibited $VEGF_{165}$-induced phosphorylation of VEGFR2, as well as the proliferation, migration, invasion and tube formation of human umbilical vascular endothelial cells. It also significantly blocked vascular formation and angiogenesis in the zebrafish model. Moreover, YL529 strongly attenuated the proliferation of A549 cells by disrupting the RAF/mitogen-activated protein (MAP) or extracellular signal-regulated kinase (Erk) kinase (MEK) kinase kinase/MAPK pathway. Oral administration of YL529 (37.5–150 $mg^{-1}{\cdot}kg^{-1}{\cdot}day^{-1}$) to nude mice bearing established tumour xenografts significantly prevented the growth (60–80%) of A549, SPC-A1, A375, OS-RC-2 and HCT116 tumours without detectable toxicity. YL529 markedly reduced microvessel density and increased tumour cell apoptosis in the tumours formed in mice inoculated with the lung cancer cells, SPC-A1 and A549, and the colon carcinoma cells, HCT116.

CONCLUSIONS AND IMPLICATIONS
YL529, an orally active multikinase inhibitor, shows therapeutic potential for solid tumours, and warrants further investigation as a possible anticancer agent.

Abbreviations
bFGF, human basic fibroblast growth factor; CADD, computer-aided drug design; CCK-8, cell count kit-8; CMC-Na, sodium carboxymethylcellulose; EDU, 5-ethynyl-2'-deoxyridine; EGM-2, endothelial growth medium-2; hpf, hour post-fertilization; HUVECs, human umbilical vascular endothelial cells; p-histone H3, phospho-histone H3; RTK, receptor tyrosine kinase; TUNEL, the terminal deoxyribonucleotidyl transferase (TDT)-mediated dUTP-digoxigenin nick end labelling; YL529, N-methyl-4-(4-(3-(trifluoromethyl)benzamido)phenoxy)picolinamide4- methylbenzenesulfonate

Introduction

Angiogenesis plays an important role in the growth of solid tumours; and inhibition of angiogenesis prevents tumour growth and/or progression in experimental models of cancer (Folkman and Beckner, 2000; Ferrara and Kerbel, 2005; Olsson *et al.*, 2006). Angiogenesis is regulated by many factors, such as VEGF and its receptors, which play important roles in regulating neovascularization and tumour angiogenesis (Ferrara *et al.*, 2003; Hicklin and Ellis, 2005). VEGF binds to transmembrane receptors expressed on vascular endothelial cells (ECs) and lymphatic vessels, and regulates numerous functions including EC migration, proliferation, protease expression, microvascular integrin expression, as well as capillary tube formation (Di Stasi *et al.*, 2008; Douglas *et al.*, 2009). The VEGFR family has five members, of which the main subtypes are VEGFR1, VEGFR2 and VEGFR3 (Zachary and Gliki, 2001; Ferrara *et al.*, 2003; Di Stasi *et al.*, 2008; Douglas *et al.*, 2009). VEGFR1-3 are exclusively located on the surface of ECs in normal tissues and are up-regulated only during embryonic and tumour angiogenesis (Cleaver and Melton, 2003; Gaengel *et al.*, 2009). Moreover, VEGFR2 is the major effector of angiogenesis and regulates blood vessel growth by activating intracellular signalling pathways that enhance the proliferation of vascular ECs (Cleaver and Melton, 2003; McCarty *et al.*, 2004; Gaengel *et al.*, 2009).

Current clinical trials have suggested that therapeutic strategies targeting tumour angiogenesis via the VEGF/VEGFR kinase axis are promising approaches for the treatment of cancer (Cristofanilli *et al.*, 2002). The RAF/MEK/MAPK pathway is one of the most important VEGF/VEGFR-activated signalling pathways (Takahashi *et al.*, 1999). In this pathway, the serine/threonine protein kinase RAF is a downstream effector of small GTPase RAS, which stimulates the proliferation, invasion and secretion of angiogenic factors. Stimulation of VEGFRs thus initiates a mitogenic kinase cascade that culminates in the phosphorylation of transcription factors that, in turn, exert profound effects on the expression of genes related to cellular proliferation and tumourigenesis (Sridhar *et al.*, 2005; Johannessen *et al.*, 2010). The functions of the RAF/MEK/MAPK pathway in many tumours depend on extracellular signals from receptor TK (RTK) at the cell surface to the nucleus via a cascade of specific phosphorylation events. This pathway thus plays a central role in regulating mammalian cell proliferation and shows great promise as a therapeutic target (Zhang *et al.*, 2009; Huynh, 2010).

Recently, small-molecule multikinase inhibitors targeting VEGFRs and RAF have been shown to have therapeutic potential in preclinical and/or clinical testing against various solid tumours (Demetri *et al.*, 2005; Sathornsumetee *et al.*, 2006), including melanoma (Eisen *et al.*, 2005), renal cell tumours (Rini *et al.*, 2005) and non-small cell lung cancer (Sandler *et al.*, 2005). For example, sorafenib, which can inhibit both VEGFRs and RAF, has been used successfully in the clinic to prolong the survival rate of hepatocarcinoma patients. However, quite a few multi-target therapies show toxicity and have only moderate response rates.

The aim of the present research was to design small-molecule multikinase inhibitors for cancer therapy, in particular, VEGFR2 and RAF kinases inhibitors, which selectively block pathological neovascularization and cancer proliferation. We previously reported the use of computer-aided drug design (CADD), *de novo* synthesis, and high-throughput screening (HTS) to identify the novel antitumour agent YL529 (Figure 1A) (Wang *et al.*, 2010). In this study, we investigated the anticancer effect and mechanism of action of YL529 *in vitro* and *in vivo*. Our results show that YL529, an inhibitor of VEGFR1, VEGFR2, VEGFR3, RAF, Fms and c-Kit, can inhibit VEGF-induced angiogenesis and induce tumour regression. YL529 will be studied in phase I clinical testing in patients with advanced solid malignancies.

The nomenclature used for receptors conforms to BJP's *Guide to Receptors and Channels* (Alexander *et al.*, 2011).

Methods

Synthesis and preparation of YL529

YL529 (N-methyl-4-(4-(3-(trifluoromethyl)benzamido) phenoxy)picolinamide4-methylbenzenesulfonate) was synthesized in the State Key Laboratory of Biotherapy, Sichuan University (Sichuan, China) and its structural formula is shown in Figure 1A. For *in vitro* assays, YL529 was dissolved in DMSO and diluted in the relevant culture media to a final DMSO concentration of 0.1% (v v^{-1}). For *in vivo* animal experiments, YL529 was suspended in 0.5% sodium carboxymethylcellulose (CMC-Na) and administered by oral gavage at volumes of 10 $mL \cdot kg^{-1} \cdot day^{-1}$.

Materials

Cell count kit-8 (CCK-8) was purchased from Dojindo (Kumamoto, Japan). DMSO and CMC-Na were purchased from Sigma Chemical Company (St. Louis, MO, USA). Human recombinant $VEGF_{165}$, human basic fibroblast growth factor (bFGF), anti-CD31 and Matrigel were purchased from BD Biosciences (San Jose, CA, USA or Amersham, UK). The primary antibodies for detection of VEGFR2, phospho (p)-VEGFR2, p44/42MAPK, p-p44/42MAPK, RAF, p-RAF, MEK, p-MEK, phospho-histone H3 (p-histone H3), as well as the HRP-conjugated secondary antibody, were purchased from Cell Signaling Technology (Beverly, MA, USA). Anti-β-actin was purchased from Santa Cruz Biotechnology (Santa Cruz, CA, USA). Anti-Ki67 was purchased from Neomarkers (Fremont, CA, USA). The TUNEL assay kit was purchased from Promega (Madison, WI, USA) and Q Tracker Red cell labelling kit from Invitrogen (Carlsbad, CA, USA). The EDU (5-ethynyl-2'-deoxyridine) detection kit was purchased from Borui Biological (Guangzhou, China). Human umbilical cord was provided by the Department of Gynecology and Obstetrics, West China Second Hospital, Sichuan University (Chengdu, China). All of the chemicals employed in the present study were of analytical grade.

Molecular docking methods

The molecular docking studies were carried out using GOLD 5.0 [Genetic Optimization of Ligand Docking, The Cambridge Crystallographic Data Centre (CCDC), Cambridge, UK]. The crystal structure of VEGFR2 (PDB ID: 3VHE) was retrieved from the RCSB Protein Data Bank and chosen as the structure of the reference protein. An 8 Å sphere around the centroid of the ligand was used to define the active site

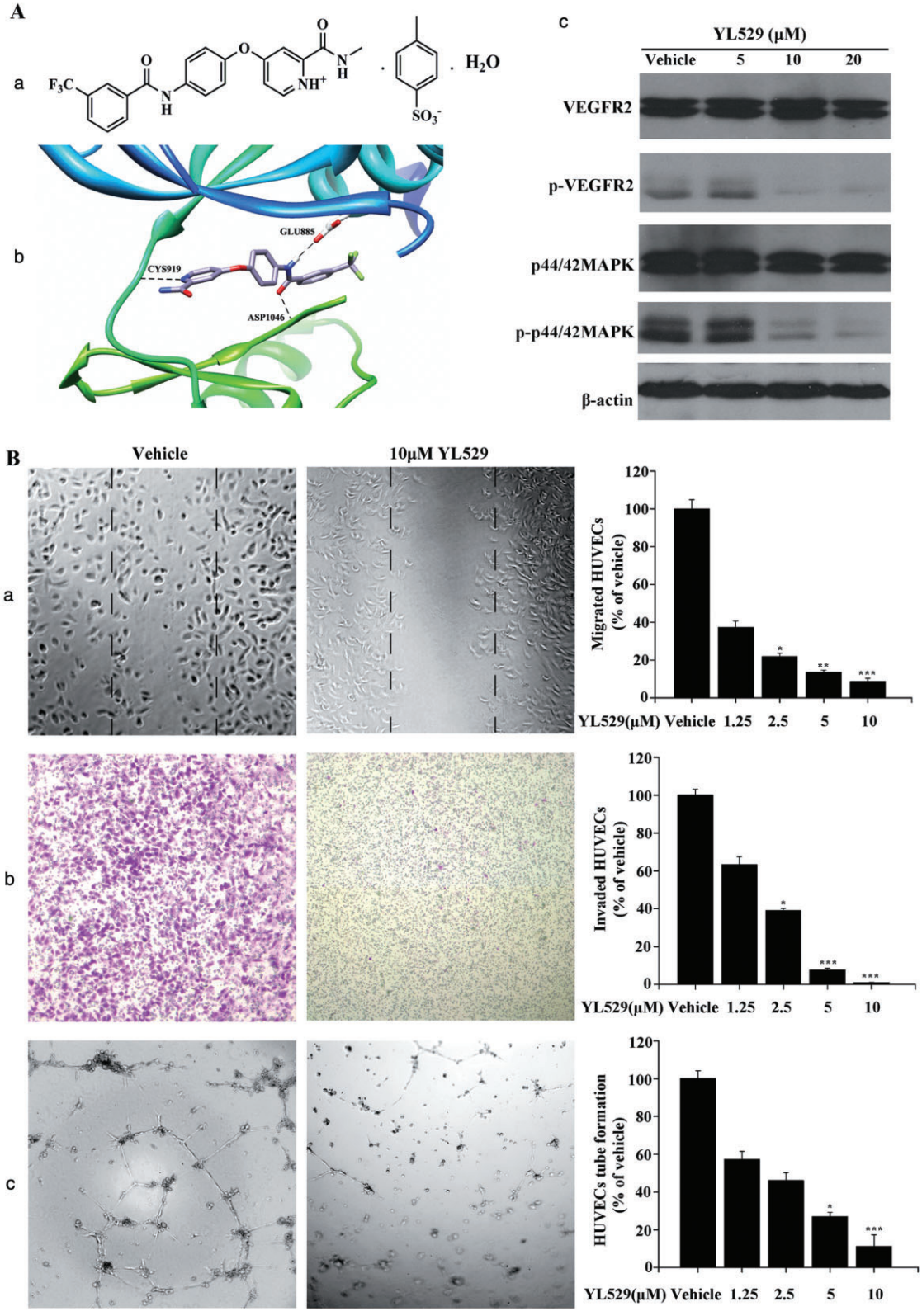

Figure 1

Chemical structure and effect of YL529 on HUVECs. (A) (a) The chemical structure of YL529 (b) YL529 was docked into the active site of VEGFR2 and the interactions between YL529 and VEGFR2 are shown in the 3-D structure. (c) $VEGF_{165}$-induced phosphorylation of VEGFR2 and p44/42MAPK in HUVECs after YL529 treatment was detected by Western blotting. (B) (a) Effects of YL529 on HUVEC migration into the wound. (b) Effects of YL529 on HUVEC invasion. (c) Effects of YL529 on HUVEC tube formation. Mean ± SEM, $n = 3$, $^{*}P < 0.05$, $^{**}P < 0.01$, $^{***}P < 0.001$.

region. The pre-process of VEGFR2 was carried out using Discovery Studio 2.55 (Accelrys, Inc., San Diego, CA, USA) software package by adding hydrogen atoms, including water removal and assigning Chemistry at HARvard Macromolecular Mechanics. YL529 was also built and its geometry was optimized in Discovery Studio 2.55. The docking scheme was modified as described previously (Cohen *et al.*, 2011).

Cell culture

SPC-A1, A549, NCI-H460 (human non-small lung carcinoma cell line), HCT-116 (human colorectal carcinoma cell line), A375 (human melanoma cell line), HeLa (human cervical carcinoma cell line), A431 (human epidermoid carcinoma cell line), HePG2, Bel-7404 (human hepatoma cell line), HEK-293 (human embryonic kidney cell line) and CT-26 (mouse colorectal carcinoma cell line) were purchased from the American Type Culture Collection (Manassas, VA, USA), and OS-RC-2 (human renal carcinoma cell line) was from the Cell Bank of Type Culture Collection of Chinese Academy of Sciences (Shanghai, China). Cells were cultured in RPMI 1640 or DMEM media supplemented with 10% FBS (Gibco, Grand Island, NY, USA), 2 mM glutamine and 1% antibiotic-antimycotic solution, and passaged 2–3 times before use. Human umbilical vein ECs (HUVECs) were isolated from human umbilical cords and cultured with endothelial growth medium-2 (EGM-2) at 37°C in a 5% CO_2 atmosphere and used 2–5 passages.

Animals

BALB/c athymic nude mice, BALB/c mice, Sprague-Dawley (SD) rats and Beagle dogs were obtained from the Beijing Animal Center (Beijing, China) and housed under controlled environmental conditions. The transgenic FLK: EGFP-zebrafish was obtained from the State Key Laboratory of Biotherapy, Sichuan University (Chengdu, China). The total numbers of animals used in these experiments were: female BALB/c nude mice, 624; female BALB/c mice, 36; female Beagle dogs, 36; male Beagle dogs, 36; male SD rats, 108; female SD rats, 60. The animals were kept at 21°C, 55% humidity, on a 12 h light (SPF)/dark cycle and had food and water available *ad libitum*. To kill the animals, they were first anaesthetized with sodium pentobarbital and then killed by exsanguination.

All of the animal protocols were reviewed and approved by the Experimental Animal Ethics Committee of Sichuan University (Chengdu, China). All studies involving animals are reported in accordance with the ARRIVE guidelines for reporting experiments involving animals (Kilkenny *et al.*, 2010; McGrath *et al.*, 2010).

Kinase assays

More than 60 human PKs were incubated with YL529 (0.001–10 μM) or vehicle in a buffer composed of 8 mM MOPS pH 7.0, 0.2 mM EDTA, 10 mM magnesium acetate, 10 μM [γ-^{33}P]-ATP and their own peptides as substrates. The reaction was initiated by the addition of the Mg-ATP mix and samples were incubated for 40 min at 25°C before the reaction was stopped by addition of 5 μL of a 3% phosphoric acid solution. The sample was then spotted onto a P30 filtermat, which was washed three times for 5 min in 75 mM phosphoric acid and once in methanol and then dried. Finally, kinase activity was detected by scintillation counting (Cao *et al.*, 2011).

Cell viability assay

Cell viability assays were performed using the CCK-8 kit according to the manufacturer's instructions. Briefly, cells were treated with YL529 for 48 h. CCK-8 was added to the cells and the plate was incubated for an additional 2–4 h. The optical density (OD) was then measured at 450 nm using a Spectra MAX M5 microplate spectrophotometer (Molecular Devices, Sunnyvale, CA, USA; Li *et al.*, 2009).

For HUVEC assays, cells were deprived of serum by incubation in solution containing 1% FBS for 12 h and incubated with YL529 for 2 h before addition of 40 ng·mL^{-1} $VEGF_{165}$ or 30 IU·mL^{-1} bFGF. Cell viability was evaluated using the CCK-8 assay after YL529 treatment for 48 h.

Scratch-induced migration assay

HUVECs and A549 cells were synchronized by in a low serum medium for 8 h, and the cell monolayers were then damaged with a micropipette to create a linear wound 2 mm in width. The indicated concentrations of YL529 (plus 4 ng·mL^{-1} $VEGF_{165}$ for HUVECs) were added and the cells were incubated for 24 h. Images were acquired using a microscope (Zeiss, Jena, Germany) and the results are expressed as the percentage inhibition rate of migration compared with untreated cells (Liang *et al.*, 2010).

Transwell migration assay

Transwell filter inserts (Billerica, MA, USA) were pre-coated with Matrigel for 30 min at 37°C. For HUVEC assays, the bottom chambers were filled with EGM-2 with or without $VEGF_{165}$ (4 ng·mL^{-1}) and the top chambers were seeded with 4×10^4 cells. For A549 cell assays, the bottom chambers were filled with RPMI 1640 supplemented with 10% FBS and the top chambers were seeded with 4×10^4 cells. Various concentrations of YL529 were added to the top and bottom chambers and the plates were incubated for 24 h. Migrated cells were stained with 0.1% crystal violet and imaged microscopically. Cells were enumerated and the results are expressed as the percentage inhibition rate of migration compared with untreated cells (Yi *et al.*, 2008).

Capillary tube formation assay

Wells of a 24-well plate were coated with Matrigel at 37°C for 45 min and 4×10^4 HUVECs were added to each well. Then, 1 mL of EGM-2 containing $VEGF_{165}$ (4 ng·mL^{-1}) and various concentrations of YL529 was added. Tube formation was assessed by microscopy after 6 h incubation and the results are expressed as the percentage inhibition rate of capillary tube formation compared with untreated cells (Cao *et al.*, 2011).

EDU incorporation assay

A549 cells were incubated with fresh medium with or without YL529 for 48 h, and proliferation was measured by incorporation of EDU into DNA using an EDU kit. The cells were examined using an inverted microscope (Zeiss) and the percentage EDU-positive cells was calculated as: %EDU-

positive cells = (EDU-positive cells, red)/(Hoechst-positive cells, blue) × 100 (Cukierman *et al.*, 2001).

Western blotting analysis

Western blotting analysis was performed by standard methods, as previously described (Lin *et al.*, 2008). HUVECs and A549 cells were deprived of serum for 10 h and then treated with YL529 for 2 h. HUVECs were treated with 50 ng·mL^{-1} $VEGF_{165}$ for 10 min. The cells were lysed and proteins were resolved by SDS-PAGE and then transferred to membranes. Proteins were detected with the appropriate primary and secondary antibodies, and the protein bands were visualized using an enhanced chemiluminescence kit (Amersham, UK).

Zebrafish angiogenesis assay

The transgenic FLK: EGFP-zebrafish embryos were maintained in Holtfreter's solution for 15 h post-fertilization (hpf). The total number of fertilised zebrafish embryos used was120. The zebrafish were kept at 28°C on a 12 h light/dark cycle and food was freely available. YL529 was added to the culture medium and images were captured using a fluorescence microscope (Zeiss) at 3 hpf (Nicoli *et al.*, 2007).

Cells of the murine tumour line B16-F10 (300 cells) were labelled with the Q Tracker kit and resuspended in Hank's balanced salt medium. Cells were directly injected into the perivitelline space of 48 hpf embryos using an air-driven Cell Tram microinjector (Medical System Corp, Green Vale, NY, USA). After 24 h, YL529 was added to the plates. Digital micrographs were taken by fluorescence microscopy after the tumour implantation.

Tumour cell-induced angiogenesis alginate model

Mouse colorectal carcinoma CT-26 cells (1×10^5) were encapsulated using alginate beads and implanted s.c. into the flanks of BALB/c mice. The mice were treated with the indicated doses of YL529 for 12 days. FITC-dextran solution (100 µL, 100 mg·kg^{-1}; Mr 150 000) was injected i.v. and 20 min later, the mice were killed, dissected and photographed. The blood content in the alginate beads was quantified by measuring the uptake of FITC-dextran into the implanted alginate beads (Hoffmann *et al.*, 1997).

Pharmacokinetic analyses

SD rats (n = 4 per group) were administered YL529 either i.v. (50 mg·kg^{-1}) or p.o. (50 mg·kg^{-1}). Blood samples were collected at appropriate intervals and the plasma concentration of YL529 was analysed by HPLC (Waters, MA, USA). The pharmacokinetic parameters were analysed using Pharmacokinetic Software of Drug and Statistics (DAS, edited and published by the Mathematical Pharmacology Professional Committee of China, Shanghai, China).

Human tumour xenograft models

Human tumour xenografts (SPC-A1, A549, A375, HCT-116 and OS-RC-2) were established by injecting cancer cells s.c. into the flanks of nude mice. When the tumour volume reached 100–300 mm^3, YL529 was administered p.o. once daily at the indicated doses. Tumour growth and animal body weights were measured every 3 days during the treatment. Tumour volumes were calculated as follows: volume (mm^3) = 0.5 × length (mm) × width^2 (mm) (Ruggeri *et al.*, 2003). At the end of the experiments, mice were killed and the organs were prepared for histopathological analysis by haematoxylin and eosin (H&E) staining.

Immunohistological and Western blotting analysis of tumours

Tumour tissues obtained from the mice bearing SPC-A1, HCT-116 and A549 tumours were subjected to immunohistological analysis. Briefly, animals (n = 8 per group) were administered YL529 p.o. for 14 days. Tumour tissues were collected and stored at −80°C for subsequent immunohistological and Western blotting analyses. TUNEL staining and immunohistological detection of anti-CD31, anti-Ki67 and p-histone H3 in tumour tissues were performed according to the manufacturers' instructions (Wedge *et al.*, 2002).

Acute toxicity study

For acute toxicity testing, male and female rats (n = 10 per group) and beagles (n = 6 per group) were administered 6000 and 5000 mg·kg^{-1} of YL529 p.o. once respectively. Clinical symptoms including mortality, clinical signs and gross findings were observed once daily for 14 days. On day 14, the rats were killed and examined by necropsy. Serum biochemistry analysis, haematological analysis and histological examinations of the major organs were carried out after dissection.

Statistical analysis

Data are expressed as the mean ± SD or SEM. SPSS (SPSS Inc., Chicago, IL, USA) software was used for statistical analysis. Statistical analyses were performed by ANOVA.

Results

Design, synthesis, screening, molecular modelling studies and kinase inhibition profile of YL529

A total of 1320 novel multikinase small-molecule compounds were designed via CADD. The 125 candidates that ranked in the top 10% according to values of the Ludi Energy Estimate 1 were chemically synthesized and screened by kinase inhibition assays (data not shown). Among the 125 tested compounds, YL529 (Figure 1Aa) was the most potent and superior to precursor compounds (Cao *et al.*, 2011; Xu *et al.*, 2011). Figure 1Ab shows the interaction modes of YL529 with the kinase domain of VEGFR2 (PDB entry 3VHE) by computer simulation and computer-based molecular docking methods. The most apparent interactions were the three hydrogen bonds formed between YL529 and VEGFR2. The first hydrogen bond was between the pyridine nitrogen and Cys^{919}, the second between the amide nitrogen and Glu^{885} and the third between the carbonyl group and Asp^{1046}.

To verify the docking results, we determined the affinity of YL529 for VEGFR2 using the SPA *in vitro* kinase binding assay. As shown in Table 1, YL529 inhibited VEGFR2 activity by 94% at 10 µM. At the same concentration, YL529 also

Table 1

In vitro profile of YL529 against a panel of kinases

Kinase	Inhibit rate at 10 μM (%)
RAF	91
VEGFR3	97
VEGFR2	94
Fms	99
Haspin	91
c-Kit	82
ErbB4	82
VEGFR1	77
PDGFRβ	48
PDGFRα	44
FGFR1	44
Aurora-A	30
Itk	6
Syk	3
LCK	3
PI3K	3
EGFR	1
IKKβ	1
CDK6/cyclinD3	0
MLK1	0
IR	0
CDK2/cyclinE	0

significantly inhibited RAF (91%), VEGFR3 (97%), Fms (99%) and c-Kit (82%) activities but did not appear to inhibit PI3K, EGF receptors, Aurora-A, CDK/cyclin or other kinases.

Effect of YL529 on HUVEC proliferation in vitro

The effect of YL529 on $VEGF_{165}$- and bFGF-stimulated growth of HUVECs was examined using the CCK-8 assay. YL529 inhibited the proliferation of HUVECs induced by $VEGF_{165}$ (40 ng·mL^{-1}), bFGF (30 U·mL^{-1}) or non-growth factors with IC_{50} values of 2.10, 5.17 and 12.89 μM respectively. These results demonstrate that YL529 can potently block VEGFR-dependent growth of HUVECs.

Effects of YL529 on VEGFR2 signalling in HUVECs

Using Western blot analysis, we investigated the effects of YL529 on VEGFR2 signalling in HUVECs. Consistent with its effect on VEGF-stimulated HUVECs' proliferation, YL529 dose-dependently blocked $VEGF_{165}$-stimulated phosphorylation of VEGFR2 (Figure 1Ac) and concomitantly inhibited the phosphorylation of p44/42 MAPK, a downstream signalling enzyme. In contrast, total levels of VEGFR2 and p44/42 MAPK were not altered by YL529 treatment.

Effects of YL529 on $VEGF_{165}$-induced HUVECs migration, invasion and tube formation

Cell migration is necessary for the function of ECs during angiogenesis and for tumour cell growth and metastasis (Shibuya, 2006). Therefore, we examined the effects of YL529 on HUVECs' migration using a $VEGF_{165}$-induced wound healing migration assay. The results showed that YL529 markedly decreased the number of HUVECs in the scratched wound in comparison to vehicle. The migration of cells treated with 1.25, 2.5, 5 and 10 μM YL529 was inhibited by 62.68, 72.04, 86.45 and 91.32%, respectively, compared with the migration of untreated cells (Figure 1Ba). These results show that YL529 can concentration-dependently inhibit the migration of $VEGF_{165}$-stimulated HUVECs.

Cell invasion is a critical function of ECs in angiogenesis (Petrovic *et al.*, 2007). To measure the effect of YL529 on HUVECs' invasion, we used a $VEGF_{165}$-induced transwell assay and measured the number of HUVECs that passed through a membrane barrier following treatment with various concentrations of YL529. As shown in Figure 1Bb, the invasion of cells treated with YL529 at 1.25, 2.5, 5 and 10 μM was inhibited by 36.54, 60.82, 88.31 and 98.90%, respectively, compared with vehicle-treated cells. These results show that YL529 can significantly inhibit the invasion of $VEGF_{165}$-stimulated HUVECs.

VEGF-induced EC tube formation is a critical step in the process of angiogenesis (Strowski *et al.*, 2003). To understand the mechanism of the anti-angiogenic effect of YL529, we measured $VEGF_{165}$-induced HUVEC tube formation. Treatment with 1–10 μM YL529 strongly inhibited VEGF-induced tube formation by 42.7 to 73.03% at concentrations between 1.25–5 μM and by 88.76% at 10 μM (Figure 1B (c)). These results indicate that YL529 potently inhibits EC migration and tube formation, supporting the results of the $VEGF_{165}$-induced HUVEC migration assay.

Effects of YL529 on tumour cell viability in vitro

To evaluate the effect of YL529 on tumour cell viability, a number of cancer cell lines was treated with YL529 for 48 h and cell viability was examined using the CCK-8 assay. As shown in Table 2, the IC_{50} of YL529 for cell viability ranged from 6 to 20 μM (Table 2), showing a remarkable inhibition of tumour cell viability. The IC_{50} was 6.19 μM for the colorectal cancer cell line HCT116, 6.68 μM for HeLa, 8.53 and 10.67 μM for SPC-A1 and A549, and 11.94 μM for the melanoma cell line. It was noteworthy that YL529 exhibited a significant safety margin on the non-cancerous human embryonic kidney cell line HEK-293. The IC_{50} for inhibition of HEK-293 cell viability was 99.2 μM, which was 12-fold higher than that for the cancer cell lines.

Effects of YL529 on A549 migration, proliferation and invasion in vitro

Cell proliferation plays an important role in cancer progression (Kawasaki *et al.*, 2001). Because inhibition of proliferation is a possible approach to cancer therapy (Huang and Houghton, 2003), we next determined the effects of YL529 on the migration, proliferation and invasion of A549 cells.

Table 2

The effects of YL529 on the viability of tumour cells

Cell line	Cell type	IC_{50} (μM)
HCT116	Human colorectal carcinoma cell line	6.19 ± 0.05
HeLa	Human cervix adenocarcinoma cell line	6.68 ± 0.03
SPC-A1	Human non-small lung cell carcinoma cell line	8.53 ± 0.07
A431	Human epidermoid carcinoma cell line	9.74 ± 0.02
OS-RC-2	Human rental carcinoma cell line	10.45 ± 0.04
A549	Human non-small lung cell carcinoma cell line	10.67 ± 0.08
NCI-H460	Human non-small lung cell carcinoma cell line	11.74 ± 0.06
A375	Human melanoma cell line	11.94 ± 0.06
HePG-2	Human hepatoma cell line	12.35 ± 0.03
Bel-7404	Human hepatoma cell line	19.06 ± 0.07

Each cell line was treated with various concentrations of YL529 for 48 h. Cell viability was examined using the CCK-8 assay and IC_{50} values are expressed as mean ± SD.

We first performed a scratch-induced migration assay. As shown in Figure 2Aa, YL529 arrested the movement of cells into the damaged region and decreased the cell number in the wound relative to the vehicle-treated cells. In cells treated with 2.5–10 μM YL529, the wounds were 26.53 and 81.35% non-confluent, respectively, indicating a striking impairment of A549 cell migration by YL529. We next assessed the effect of YL529 on A549 cell invasion using transwell assay. As shown in Figure 2Ab, YL529 treatment for 48 h significantly decreased the number of A549 cells invading the wound compared with vehicle-treated cells. Cell invasion was inhibited by 29.96, 46.82, 76.03 and 86.89% in the presence of 2.5, 5, 10 and 20 μM YL529 respectively. These data indicate YL529 significantly inhibits the invasion of A549 cells.

We used the EDU-DNA incorporation assay to evaluate the anti-proliferative effect of YL529 on A549 cells. As shown in Figure 2Ac, the percentage of cells in the S-phase was reduced by 30.62, 35.64, 69.2 and 85.99%, following treatment with 2.5, 5, 10, and 20 μM YL529 respectively. These results indicate that YL529 can inhibit the proliferation of A549 cells in a concentration-dependent manner.

YL529 inhibited the RAF/MEK/MAPK signalling pathway in A549 cells

In the kinase activity assays, we found that YL529 significantly inhibited the activity of RAF (Table 1). To gain further insight into the molecular mechanism of this anti-proliferative effect of YL529, the expression levels of RAF, MEK and p44/42 MAPK were investigated by Western blotting. As shown in Figure 2B, YL529 potently inhibited the phosphorylation of RAF, MEK and 44/42 MAPK. In addition, YL529 decreased the expression of p-histone H3, suggesting the formation of condensed chromosomes after YL529 exposure.

YL529 inhibited tumour angiogenesis in mice and zebrafish models

The anti-angiogenic effect of YL529 was examined using mice and zebrafish models; and immunohistochemical analysis was conducted using tissues derived from tumour-bearing mice. Tumours from the animals treated with 150 $mg \cdot kg^{-1} \cdot day^{-1}$ YL529 showed a vessel density 7.63% (SPC-A1) and 5.94% (HCT116) less than in those from vehicle-treated animals, suggesting that YL529 significantly decreases the density of microvessels in tumours (Figure 3A).

In the CT-26 cell-induced angiogenesis alginate model, a dose-dependent anti-angiogenic effect was observed after oral administration of YL529 for 12 days in mice. As shown in Figure 3B, the accumulation of FITC-dextran in vehicle alginate was 3.04 μg·per alginate; however, the accumulation of FITC-dextran was markedly decreased in animals treated with 37.5 or 75 $mg \cdot kg^{-1} \cdot day^{-1}$ YL529. Maximal inhibition was observed in animals treated with 150 $mg \cdot kg^{-1} \cdot day^{-1}$ YL529, in which the accumulation of FITC-dextran was 0.92 μg per·alginate and microvessel density was reduced by 69.70%.

We also examined the anti-angiogenic effect of YL529 using a zebrafish model. During zebrafish embryonic development, the intersegmental vessels (ISV) sprouting begins at 10 hpf and reaches its highest density at 30 hpf. YL529 administration was started at 15 hpf and we detected the ISV at 30 hpf. We found that the ECs in the YL529 treatment group did not migrate into the intersomitic region to form complete vessels (Figure 3C). The length of the ISV was 84.98 μm in vehicle-treated animals and this was reduced to 40.28 μm after treatment with 2.5 μM YL529. These results demonstrate that YL529 significantly inhibits zebrafish ISV formation. YL529 also inhibited B16-F10 cell-induced angiogenesis in zebrafish. As shown in Figure 3D, ECs filled the inner space of the B16-F10 tumour xenograft in the vehicle-treated group and a primary vascular network was visible 5 days after implantation of the tumour into the zebrafish. However, the vascular network was clearly inhibited in the embryos treated with 2.5 μM YL529, in which the tumour volume and vessel length were only ~14 and 33% of those in the vehicle-treated group. Taken together, these *in vivo* results indicate that YL529 possesses a notable anti-angiogenic activity, which is consistent with its effects on HUVEC proliferation *in vitro*.

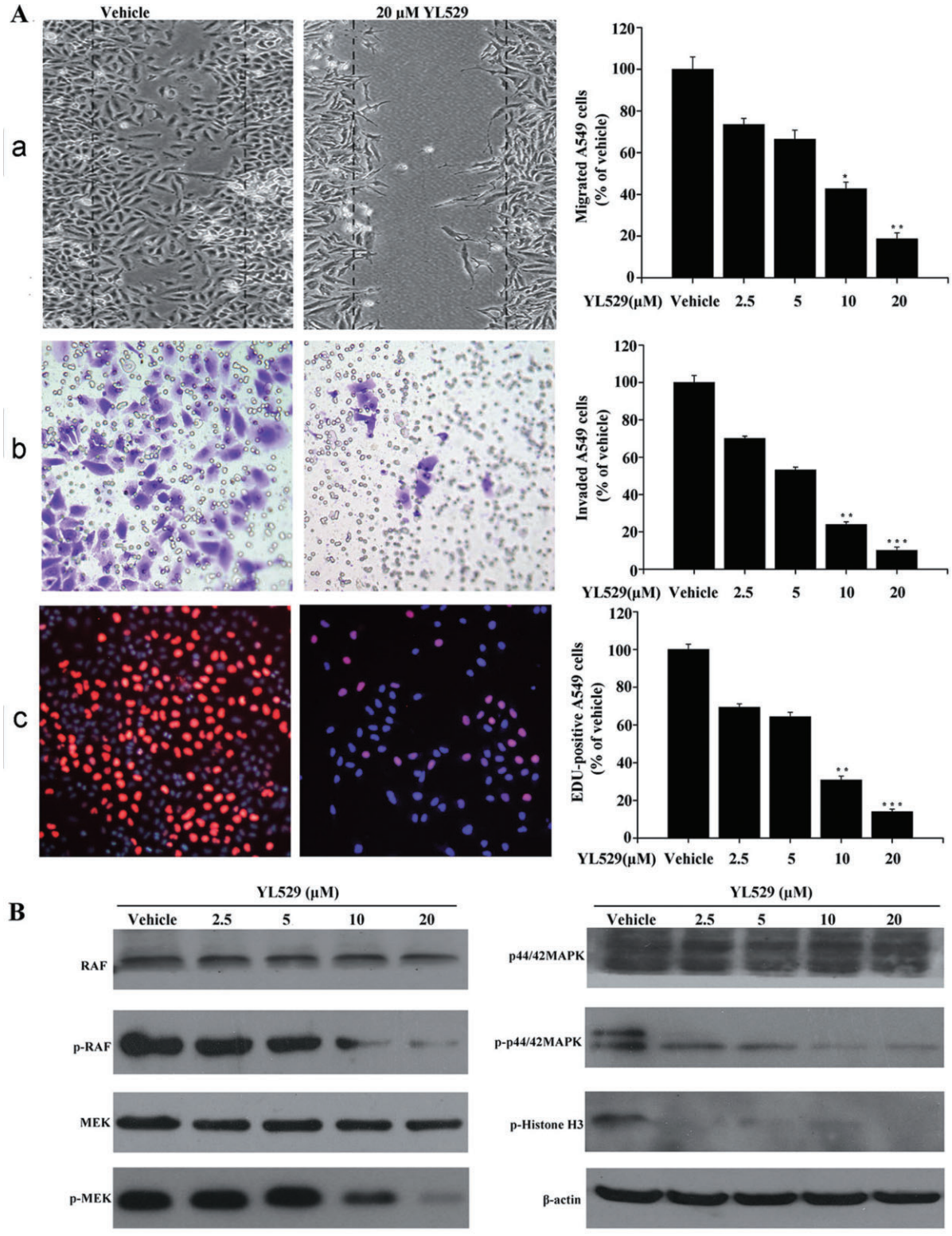

Figure 2

Anti-proliferative effects of YL529 on A549 cells *in vitro*. (A) YL529 inhibited A549 cell proliferation, migration and invasion *in vitro*. (a) Effects of YL529 on A549 cell migration in wound migration assays (40×). (b) Effects of YL529 on A549 cell invasion using transwell assays (100×). (c) YL529 inhibited the proliferation of A549 cells in a concentration-dependent manner in the EDU assay. The panels shown are representative fields of EDU-positive (red) and Hoechst 33358 (blue) staining (100×). Quantification was shown on the right of the panels respectively. Results are percentage inhibition rate versus untreated wells. Mean ± SEM, $n = 3$, $^{*}P < 0.05$, $^{**}P < 0.01$. (B) YL529 inhibited the expression of p-RAF and the downstream signalling pathway *in vitro*. Western blotting analysis showed the expressions of phosphorylated and total RAF, p44/42 MAPK and MEK.

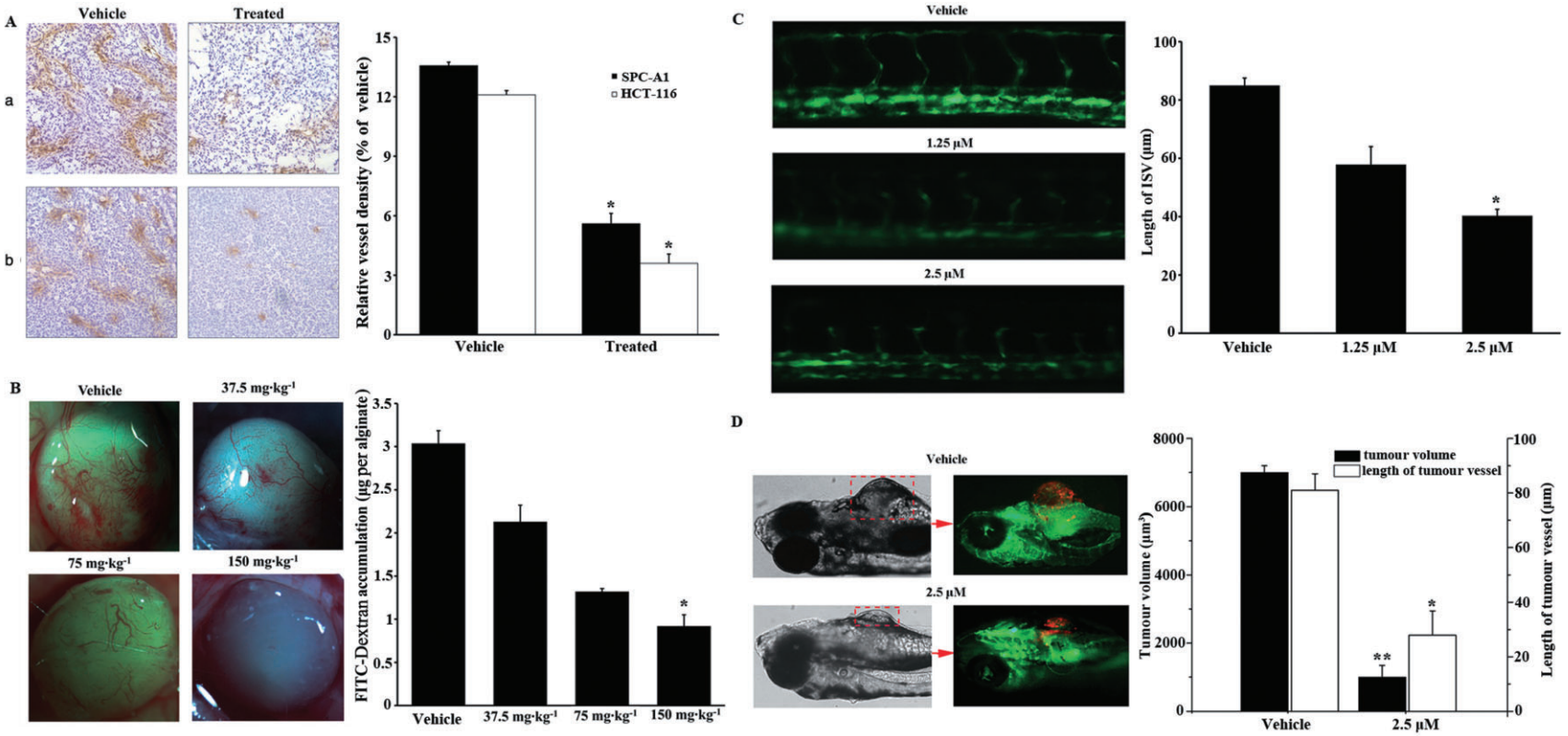

Figure 3

Effects of YL529 on angiogenesis *in vivo*. (A) YL529 significantly inhibited tumour microvessels in SPC-A1 and HCT-116 tumour xenografts, shown with CD31 staining. Mean ± SEM, $n = 8$, 200×, $^{*}P < 0.05$, $^{**}P < 0.01$. (B) YL529 inhibited angiogenesis of mice implanted with alginate beads containing CT-26 cells. The uptake of FITC-dextran was quantified after YL529 treatment. Each experiment was performed three times. Mean ± SEM, $n = 6$, 40×, $^{*}P < 0.05$, $^{**}P < 0.01$. (C) Fluorescence images of 30 hpf zebrafish treated with YL529. Mean ± SEM, $n = 10$, 40×, $^{*}P < 0.05$. (D) YL529 greatly inhibited murine melanoma cell B16-F10-induced angiogenesis in zebrafish. Each experiment was performed three times. Mean ± SEM, $n = 5$, 40×, $^{*}P < 0.05$, $^{**}P < 0.01$.

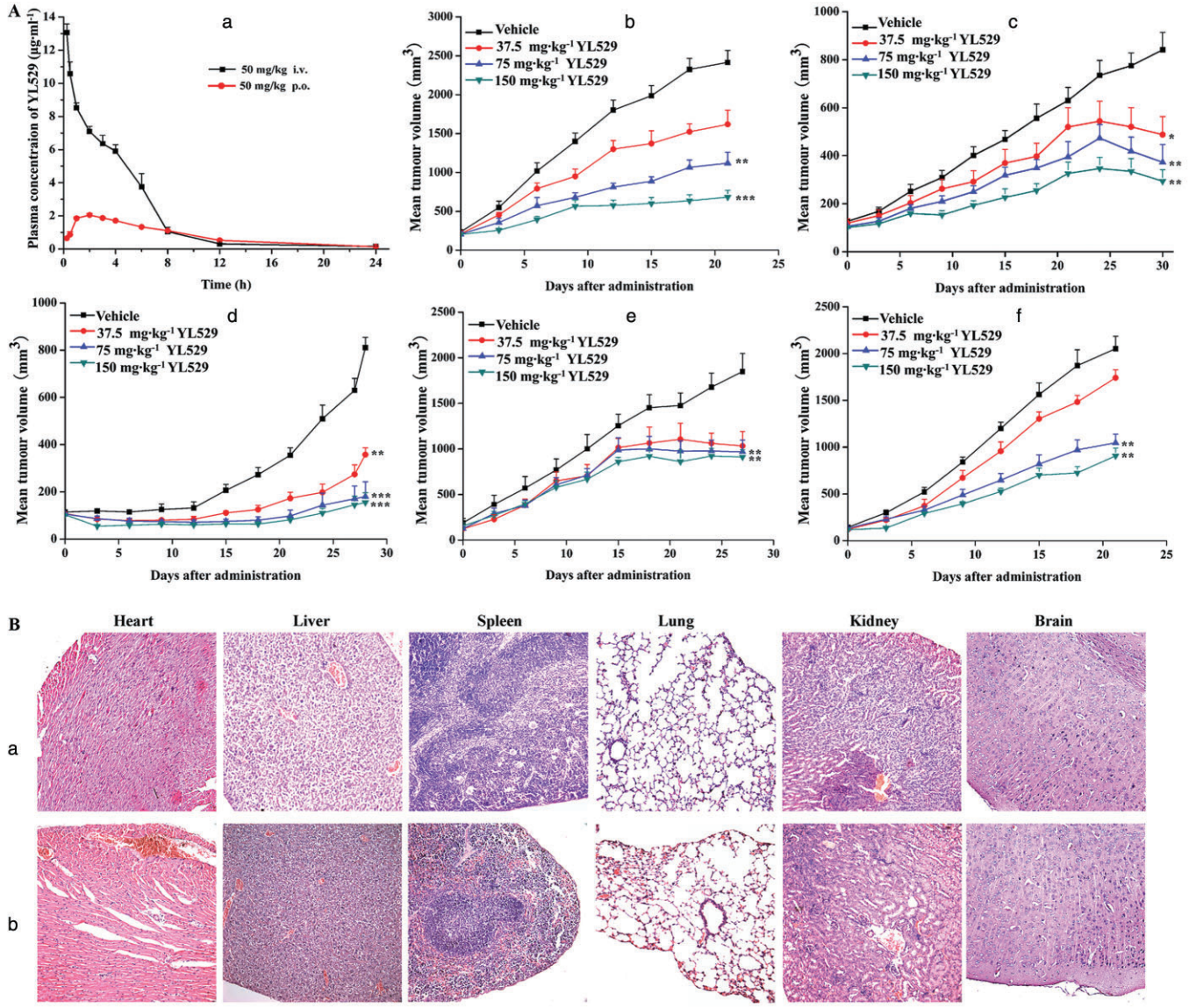

Figure 4

Anticancer activity of YL529 *in vivo*. (A) (a) The concentration-time curve of YL529 *in vivo:* SD rats were administered 50 mg·kg^{-1} YL529 i.v. or p.o. Blood samples were collected at the indicated intervals after YL529 administration and the concentration of YL529 was determined by HPLC. (B) Mice bearing SPC-A1 (b), A549 (c), HCT-116 (d), A375 (e) and OS-RC-2 (f) tumours were treated with YL529 and body weights were determined ($n = 8$) (*$P < 0.05$, **$P < 0.01$, ***$P < 0.001$). (B) YL529 did not cause pathological abnormalities in mice. Tissues were stained with H&E. (a) Vehicle- and (b) 150 mg·kg^{-1} YL529-treated group of mice bearing SPC-A1 tumours. ($n = 8$, 100×).

Pharmacokinetics of YL529 in vivo

To determine the pharmacokinetic characteristics of YL529, SD rats were administered YL529 p.o. or i.v. and the plasma concentration of YL529 was measured by HPLC. The pharmacokinetic profiles of YL529 are summarized in Figure 4Aa. After i.v. administration of 50 mg·kg^{-1} YL529, the elimination of half-life ($t_{1/2}$) was 2.33 h, $AUC_{0\to\infty}$ was 30.69 mg·L^{-1}·h. After p.o. administration of 50 mg·kg^{-1} YL529, the peak plasma concentration (C_{max}) was 1.18 μg·mL^{-1}, the time-to-peak concentration 2.67 h, the $t_{1/2}$ 5.77 h and the $AUC_{0\to\infty}$ 12.20 mg·L^{-1}·h. The bioavailability of YL529 in rats was determined to be 39.75%.

Antitumour activity of YL529 in vivo

To study the antitumour effects of YL529 *in vivo*, SPC-A1, A549, A375, HCT-116 and OS-RC-2 tumour-bearing nude mice were administered YL529 p.o. at doses of 37.5, 75, or 150 mg·kg^{-1}·day^{-1}. As shown in Figure 4Ab–f, tumour volumes in mice treated with 150 mg·kg^{-1}·day^{-1} YL529 for 18–30 days were inhibited by 71.75% (SPC-A1), 73.48% (A549), 78.31% (A375), 55.84% (HCT-116) and 55.80% (OS-RC-2), respectively, compared with the vehicle-treated groups. In addition, there was no loss of body weight (Supporting Information Figure S1), and no lesion was observed in the heart, liver, spleen, lung, kidney and brain of

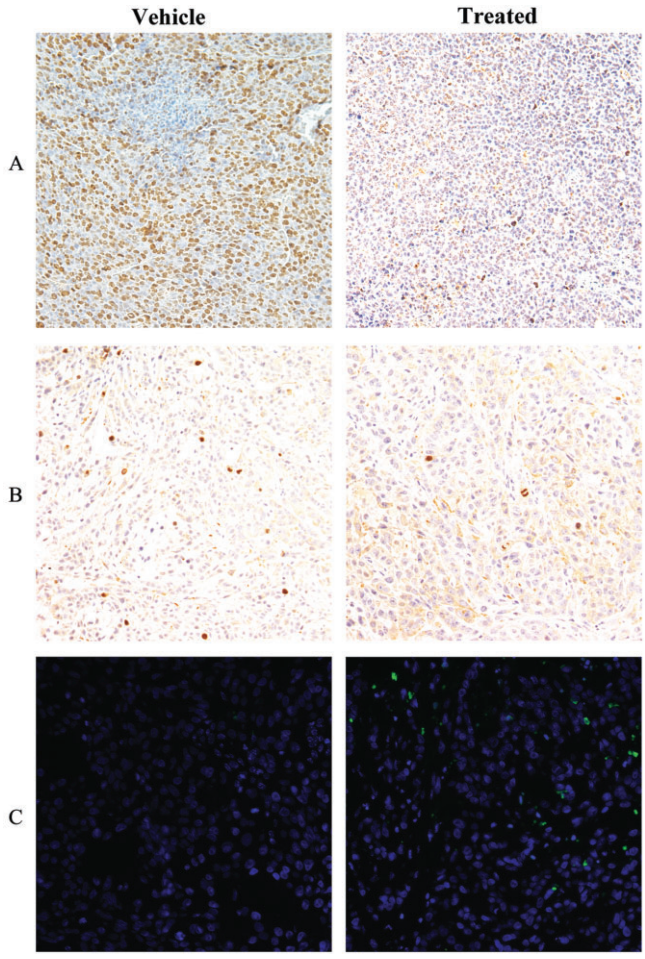

Figure 5

Effects of YL529 on proliferation and apoptosis *in vivo*. The anti-proliferative and pro-apoptotic effects of YL529 were determined in the A549 tumour model. (A) Ki67 ($n = 8$, 200×), (B) phospho-histone H3 ($n = 8$, 200×) and (C) TUNEL were detected in the A549 tumour xenograft model.

YL529-treated mice, suggesting that YL529 treatment was well tolerated (Figure 4B).

We conducted immunohistochemical analysis and a TUNEL apoptosis assay to evaluate whether YL529 could inhibit the proliferation and induce tumour cell apoptosis *in vivo*. As shown in Figure 5A and B, YL529 markedly decreased the number of proliferating A549 cells in tumour tissues after YL529 treatment for 14 days, as indicated by the cell cycle markers Ki67 (5% vs. vehicle) and p-histone H3 (10% vs. vehicle), showing it has a strong inhibitory effect on tumour cell proliferation *in vivo*. Moreover, a strong fluorescence signal was observed in the nuclei of tumour cells derived from mice treated with 150 mg·kg^{-1} YL529 (16-fold increase vs. vehicle), indicating the presence of a large number of apoptotic cells (Figure 5C).

Safety profile of YL529 in a preclinical study

As mentioned above, mice treated with YL529 for 18–30 days showed no body weight loss or tissue damage. To further investigate the safety profile of YL529, we conducted an acute toxicity test in SD rats (6000 mg·kg^{-1}) and beagle dogs (5000 mg·kg^{-1}). Mortality, clinical signs and body weights of the animals were monitored over a 14-day post-dose period. Importantly, no obvious changes were observed; these included data for serum biochemistry, haematology and histopathology (Figure 6, Supporting Information Tables S1 and S2). As no adverse effects of YL529 were observed at doses of 6000 mg·kg^{-1} in rats and 5000 mg·kg^{-1} in dogs, it is assumed YL529 has a high safety profile.

Discussion and conclusions

Tumour cell angiogenesis and proliferation are critical processes in the growth of solid tumours (Carmeliet *et al.*, 1998). Targeting these processes with small-molecule RTK inhibitors has been demonstrated to be an effective approach for human cancer treatment (Zou *et al.*, 2007; Le Tourneau *et al.*, 2008). In the present study, we demonstrated that YL529 selectively inhibits the activity of VEGFR2, VEGFR3, RAF, Fms and c-Kit *in vitro* and significantly inhibits the progression of human cancer cell growth both *in vitro* and *in vivo* without significant toxicity. Moreover, YL529 has a novel chemical structure that is different from VEGFR inhibitors in clinical use. In the present study, we describe the biochemical, pharmacological and toxicological profiles of YL529.

Among the various types of RTKs, the VEGF/VEGFR pathway has been widely studied because VEGFR expression is strongly correlated with tumour progression and poor prognosis. Therefore, this pathway has been pursued as a therapeutic strategy for inhibition of angiogenesis and neovascular survival in tumours (Kiselyov *et al.*, 2007; Suzuki *et al.*, 2008). YL529 was developed as a potential anticancer agent in our laboratory using CADD, HTS and *de novo* synthesis. The *in vitro* kinase assay showed that YL529 effectively inhibited the activity of VEGFR2 and VEGFR3. The VEGF–VEGFR2 interaction stimulates EC proliferation, migration, invasion, tube formation and angiogenesis. Furthermore, VEGF signalling and angiogenesis in ECs is mainly mediated through VEGFR2. We investigated the anti-angiogenic effect of YL529 on HUVECs *in vitro* and found that YL529 significantly inhibited VEGF-stimulated proliferation of HUVECs. The mouse tumour cell-containing alginate bead model and zebrafish angiogenesis model have emerged as exceptionally useful models for the study of anti-angiogenic reagents (Hoffmann *et al.*, 1997; Kari *et al.*, 2007). We confirmed the anti-angiogenic effect of YL529 using these *in vivo* models. Collectively, our results indicate that YL529 can dose-dependently inhibit the angiogenic response in an alginate implant model in mice and ISV development in zebrafish. Besides stimulating tumour vascularization, the VEGF–VEGFR interactions are also responsible for tumour cell migration and invasion. VEGFR3, which binds the homologues VEGFC and VEGFD, has a critical role in lymphangiogenesis, and a prognostic link between the expression of VEGFC and/or VEGFD and nodal metastasis has been identified for several tumour types (Nathanson, 2003). Therefore, direct inhibition of VEGFR3 signalling may have a therapeutic benefit in limiting subsequent tumour cell dissemination. YL529 may inhibit tumour cell migration and invasion by

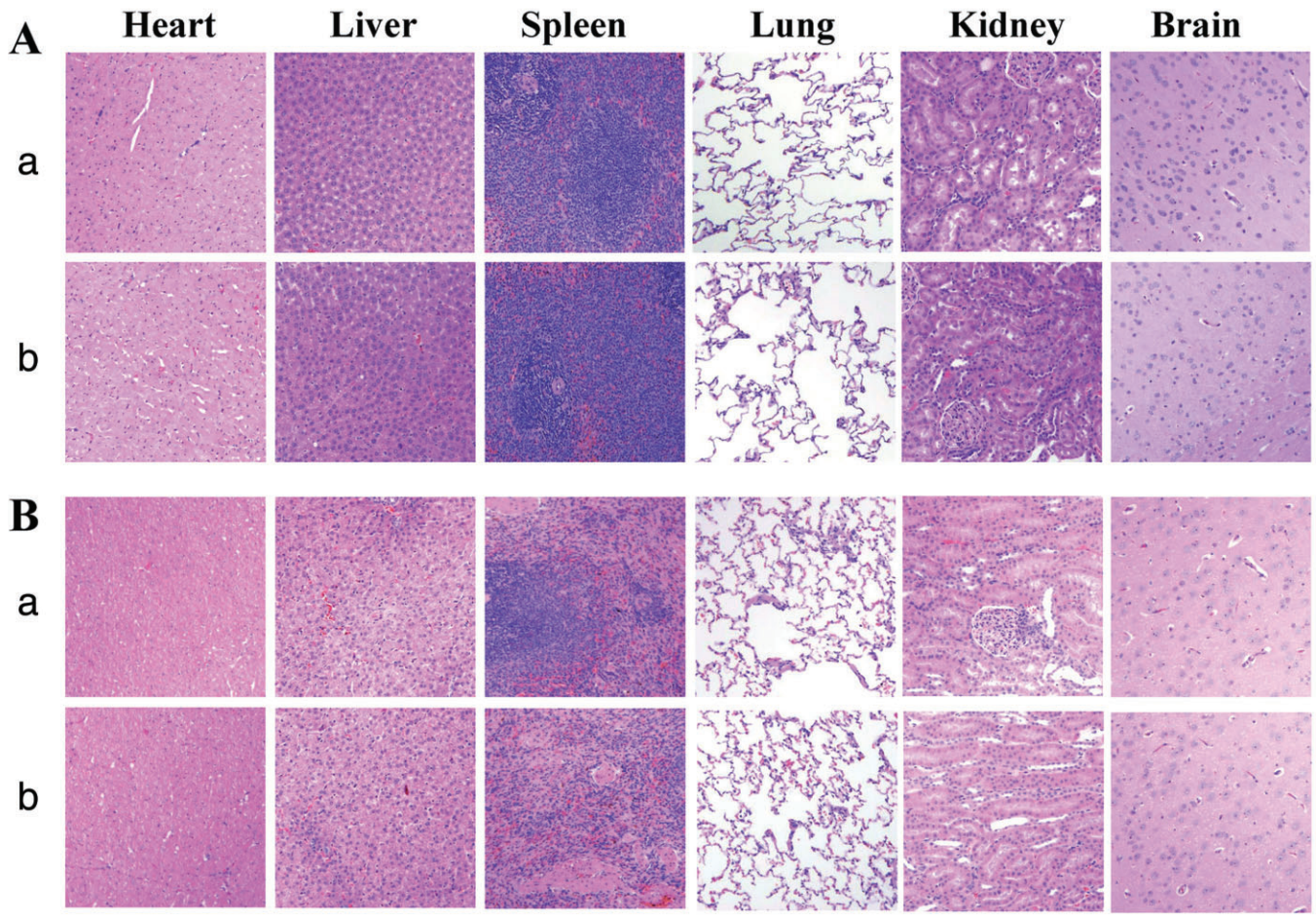

Figure 6

Safety profile of YL529 *in vivo*. YL529 did not cause pathological abnormalities in rat and Beagle tissues in acute toxicity tests. Tissues from (A) rats and (B) Beagles were stained with H&E. (a) Vehicle- and (b) 150 mg·kg^{-1} YL529-treated groups (n = 10 for rats, n = 6 for Beagles, 100×).

inhibiting both VEGFR2 and VEGFR3 signalling. YL529 also strongly inhibited migration of $VEGF_{165}$-induced HUVECs and invasion of A549 cells. In addition to VEGFR2 and VEGFR3, an evaluation of more than 60 kinases revealed that YL529 also inhibited the activities of RAF, c-Kit and Fms but without blocking other protein kinases such as PI3K and cyclin-dependent kinases. These results indicate that YL529, a multikinase inhibitor, can significantly inhibit the activities of VEGFR2, VEGFR3, RAF, c-Kit and Fms. In our previous cell-based screening study of anticancer drugs, it was revealed that YL529 exhibits antitumour activity against various kinds of cancer cell lines with IC_{50} values ranging from 6 to 20 μM. Moreover, YL529 inhibited the proliferation of A549 cells in a concentration-dependent manner and exhibited a notable effect in the EDU assay. These results are consistent with the findings of the kinase assay, indicating that YL529 is capable of inhibiting both angiogenesis and tumour cell proliferation. Targeting RAF kinases is an important concept for cancer therapy because the RAF kinase family is a component of the Ras/RAF/MEK/ERK oncogenic signalling pathway. The involvement of this pathway in tumour cell proliferation and tumour progression is well documented (Lang *et al.*, 2008). YL529 significantly inhibits RAF, indicating that RAF is a potential target for YL529-mediated tumour suppression. YL529 also attenuated the expression levels of p-RAF, p-MEK and p-44/42 MAPK in A549 cells. Taken together, these results suggest that YL529 is capable of blocking the RAF/MEK/ERK signalling pathway, an important pathway for tumour progression and angiogenesis (Wilhelm *et al.*, 2004; Thompson and Lyons, 2005). As YL529 was found to disrupt the pro-angiogenic signalling cascades in both tumour cells and ECs, as well as diminish the pro-migratory properties of cancer cells, it is considered to be a multikinase anticancer agent with both anti-angiogenic and anti-proliferative effects.

c-Kit, a member of the type III receptor TK family, is expressed in some human tumours (Turner *et al.*, 1992). It has been reported that the down regulation of c-Kit has an anti-proliferative effect in human tumours (Hirota *et al.*, 1998; Kijima *et al.*, 2002; Growney *et al.*, 2005). Fms is a TK closely related to VEGFR3 and VEGFR1. Our results showed that c-Kit and Fms, together with other closely related members of this kinase family like VEGFR1, VEGFR2 and VEGFR3, were inhibited by YL529. Thus, inhibition of c-Kit and Fms may con-

tribute to the effect of YL529 in preventing tumour cell proliferation and angiogenesis.

Because not all compounds exhibiting antitumour activity *in vitro* show anticancer activity *in vivo*, we also investigated the antitumour effect of YL529 in several human tumour xenograft models in athymic mice. These models have been used for the determination of the pharmacodynamics and mechanism of action of small-molecule drugs *in vivo* (Uchida *et al.*, 2001; Ruggeri *et al.*, 2003; Dev *et al.*, 2004; Wu *et al.*, 2004). The most marked inhibitory effect of YL529 was observed in SPC-A1 and A375 tumour models. The effective dose range of YL529 in the nude mice models was between 37.5 and 75 $mg \cdot kg^{-1} \cdot day^{-1}$. Moreover, YL529 treatment for 14 days reduced microvessel density and tumour cell proliferation.

In an acute toxicity evaluation, we found that YL529 exhibited no toxicity in rats and dogs. Chronic toxicity tests (6 months) in rats and dogs are ongoing and, so far, after 3-months of YL529 administration, no obvious changes in clinical signs and body weights of animals have been observed. In contrast, for the VEGFR inhibitor sorafenib, the maximum tolerated dose in acute toxicity test in rats was found to be 500 $mg \cdot kg^{-1}$, which is much lower than that of YL529 (http://www.accessdata.fda.gov/scripts/cder/drugsatfda). Moreover, a single dose of sorafenib can induce toxic effects in the gastrointestinal tract and on liver function. However, our results show that YL529 has a good safety profile.

In summary, our results indicate that YL529, a potent and orally active multi-target kinase inhibitor, possesses anti-angiogenic and anti-proliferative effects against solid tumours. YL529 may provide a relatively non-toxic adjuvant therapy for cancer and has great potential for drug development and clinical application in the future.

Acknowledgements

This work is supported by the National Science & Technology Major project (2011ZX09102-001-013 and 2012ZX09501-003), Program for New Century Excellent Talents in University and the Project of the National Natural Sciences Foundation of China (81272459).

Conflicts of interest

None.

References

Alexander SPH, Mathie A, Peters JA (2011). Guide to receptors and channels (GRAC), 5th Edition. Br J Pharmacol 164 (Suppl. 1): S1–S324.

Cao ZX, Zheng RL, Lin HJ, Luo SD, Zhou Y, Xu YZ *et al.* (2011). SKLB610: a novel potential inhibitor of vascular endothelial growth factor receptor tyrosine kinases inhibits angiogenesis and tumor growth *in vivo*. Cell Physiol Biochem 27: 565–574.

Carmeliet P, Dor Y, Herbert JM, Fukumura D, Brusselmans K, Dewerchln M *et al.* (1998). Role of HIF-1 in hypoxia-mediated apoptosis, cell proliferation and tumour angiogenesis. Nature 394: 485–490.

Cleaver O, Melton DA (2003). Endothelial signaling during development. Nat Med 9: 661–668.

Cohen F, Bergeron P, Blackwood E, Bowman KK, Chen H, DiPasquale AG *et al.* (2011). Potent, selective, and orally bioavailable inhibitors of mammalian target of rapamycin (mTOR) kinase based on a quaternary substituted dihydrofuropyrimidine. J Med Chem 54: 3426–3435.

Cristofanilli M, Charnsangavej C, Hortobagyi GN (2002). Angiogenesis modulation in cancer research: novel clinical approaches. Nat Rev Drug Discov 1: 415–426.

Cukierman E, Pankov R, Stevens DR, Yamada KM (2001). Taking cell-matrix adhesions to the third dimension. Science 294: 1702–1708.

Demetri G, Van Oosterom A, Blackstein M, Garrett C, Shah M, Heinrich M *et al.* (2005). Phase 3, multicenter, randomized, double-blind, placebo-controlled trial of SU11248 in patients (pts) following failure of imatinib for metastatic GIST. J Clin Oncol 23 (16_Suppl.): 4000.

Dev I, Dornsife R, Hopper T, Onori J, Miller C, Harrington L *et al.* (2004). Antitumour efficacy of VEGFR2 tyrosine kinase inhibitor correlates with expression of VEGF and its receptor VEGFR2 in tumour models. Br J Cancer 91: 1391–1398.

Di Stasi R, Capasso D, Diana D, Fattorusso R, Pedone C, D'Andrea LD (2008). Vascular endothelial growth factor (VEGF) and its receptors: key regulators of angiogenesis. J Pept Sci 14: 174–174.

Douglas NC, Tang HY, Gomez R, Pytowski B, Hicklin DJ, Sauer CM *et al.* (2009). Vascular endothelial growth factor receptor 2 (VEGFR-2) functions to promote uterine decidual angiogenesis during early pregnancy in the mouse. Endocrinology 150: 3845–3854.

Eisen T, Ahmad T, Gore M, Marais R, Gibbens I, James M *et al.* (2005). Phase I trial of BAY 43-9006 (sorafenib) combined with dacarbazine (DTIC) in metastatic melanoma patients. J Clin Oncol 23 (16 Suppl.): 7508.

Ferrara N, Kerbel RS (2005). Angiogenesis as a therapeutic target. Nature 438: 967–974.

Ferrara N, Gerber H, LeCouter J (2003). The biology of VEGF and its receptors. Nat Med 9: 669–676.

Folkman J, Beckner K (2000). Angiogenesis imaging. Acad Radiol 7: 783–785.

Gaengel K, Genove G, Armulik A, Betsholtz C (2009). Endothelial-mural cell signaling in vascular development and angiogenesis. Arterioscl Throm Vas Biol 29: 630–638.

Growney JD, Clark JJ, Adelsperger J, Stone R, Fabbro D, Griffin JD *et al.* (2005). Activation mutations of human c-KIT resistant to imatinib mesylate are sensitive to the tyrosine kinase inhibitor PKC412. Blood 106: 721–724.

Hicklin DJ, Ellis LM (2005). Role of the vascular endothelial growth factor pathway in tumor growth and angiogenesis. J Clin Oncol 23: 1011–1027.

Hirota S, Isozaki K, Moriyama Y, Hashimoto K, Nishida T, Ishiguro S *et al.* (1998). Gain-of-function mutations of c-kit in human gastrointestinal stromal tumors. Science 279: 577–580.

Hoffmann J, Schirner M, Menrad A, Schneider MR (1997). A highly sensitive model for quantification of in vivo tumor angiogenesis induced by alginate-encapsulated tumor cells. Cancer Res 57: 3847–3851.

Huang S, Houghton PJ (2003). Targeting mTOR signaling for cancer therapy. Curr Opin Pharmacol 3: 371–377.

Huynh H (2010). Molecularly targeted therapy in hepatocellular carcinoma. Biochem Pharmacol 80: 550–560.

Johannessen CM, Boehm JS, Kim SY, Thomas SR, Wardwell L, Johnson LA *et al*. (2010). COT drives resistance to RAF inhibition through MAP kinase pathway reactivation. Nature 468: 968–972.

Kari G, Rodeck U, Dicker AP (2007). Zebrafish: an emerging model system for human disease and drug discovery. Clin Pharmacol Ther 82: 70–80.

Kawasaki H, Toyoda M, Shinohara H, Okuda J, Watanabe I, Yamamoto T *et al*. (2001). Expression of survivin correlates with apoptosis, proliferation, and angiogenesis during human colorectal tumorigenesis. Cancer 91: 2026–2032.

Kijima T, Maulik G, Ma PC, Tibaldi EV, Turner RE, Rollins B *et al*. (2002). Regulation of cellular proliferation, cytoskeletal function, and signal transduction through CXCR4 and c-Kit in small cell lung cancer cells. Cancer Res 62: 6304–6311.

Kilkenny C, Browne W, Cuthill IC, Emerson M, Altman DG (2010). NC3Rs Reporting Guidelines Working Group. Br J Pharmacol 160: 1577–1579.

Kiselyov A, Balakin KV, Tkachenko SE (2007). VEGF/VEGFR signalling as a target for inhibiting angiogenesis. Expert Opin Inv Drug 16: 83–107.

Lang SA, Brecht I, Moser C, Obed A, Batt D, Schlitt HJ *et al*. (2008). Dual inhibition of Raf and VEGFR2 reduces growth and vascularization of hepatocellular carcinoma in an experimental model. Langenbeck Arch Surg 393: 333–341.

Le Tourneau C, Faivre S, Raymond E (2008). New developments in multitargeted therapy for patients with solid tumours. Cancer Treat Rev 34: 37–48.

Li ZG, Zhao YL, Wu XH, Ye HY, Peng AH, Cao ZX *et al*. (2009). Barbigerone, a natural isoflavone, induces apoptosis in murine lung-cancer cells via the mitochondrial apoptotic pathway. Cell Physiol Biochem 24: 95–104.

Liang S, Fu A, Zhang Q, Tang M, Zhou J, Wei Y *et al*. (2010). Honokiol inhibits HepG2 migration via down-regulation of IQGAP1 expression discovered by a quantitative pharmaceutical proteomic analysis. Proteomics 10: 1474–1483.

Lin LG, Xie H, Li HL, Tong LJ, Tang CP, Ke CQ *et al*. (2008). Naturally occurring homoisoflavonoids function as potent protein tyrosine kinase inhibitors by c-Src-based high-throughput screening. J Med Chem 51: 4419–4429.

McCarty M, Wey J, Stoeltzing O, Liu W, Fan F, Bucana C *et al*. (2004). ZD6474, a vascular endothelial growth factor receptor tyrosine kinase inhibitor with additional activity against epidermal growth factor receptor tyrosine kinase, inhibits orthotopic growth and angiogenesis of gastric cancer. Mol Cancer Ther 3: 1041–1048.

McGrath J, Drummond G, McLachlan E, Kilkenny C, Wainwright C (2010). Guidelines for reporting experiments involving animals: the ARRIVE guidelines. Br J Pharmacol 160: 1573–1576.

Nathanson SD (2003). Insights into the mechanisms of lymph node metastasis. Cancer 98: 413–423.

Nicoli S, Ribatti D, Cotelli F, Presta M (2007). Mammalian tumor xenografts induce neovascularization in zebrafish embryos. Cancer Res 67: 2927–2931.

Olsson AK, Dimberg A, Kreuger J, Claesson-Welsh L (2006). VEGF receptor signalling-in control of vascular function. Nat Rev Mol Cell Biol 7: 359–371.

Petrovic N, Schacke W, Gahagan JR, O'Conor CA, Winnicka B, Conway RE *et al*. (2007). CD13/APN regulates endothelial invasion and filopodia fonnation. Blood 110: 142–150.

Rini B, Rixe O, Bukowski R, Michaelson M, Wilding G, Hudes G *et al*. (2005). AG-013736, a multi-target tyrosine kinase receptor inhibitor, demonstrates anti-tumor activity in a Phase 2 study of cytokine-refractory, metastatic renal cell cancer (RCC). J Clin Oncol 23 (16_Suppl.): 4509.

Ruggeri B, Singh J, Gingrich D, Angeles T, Albom M, Chang H *et al*. (2003). CEP-7055: a novel, orally active pan inhibitor of vascular endothelial growth factor receptor tyrosine kinases with potent antiangiogenic activity and antitumor efficacy in preclinical models. Cancer Res 63: 5978–5991.

Sandler A, Gray R, Brahmer J, Dowlati A, Schiller J, Perry M *et al*. (2005). Randomized phase II/III Trial of paclitaxel (P) plus carboplatin (C) with or without bevacizumab (NSC# 704865) in patients with advanced non-squamous non-small cell lung cancer (NSCLC): an Eastern Cooperative Oncology Group (ECOG) Trial-E4599. J Clin Oncol 23 (16_Suppl.): LBA4.

Sathornsumetee S, Hjelmeland AB, Keir ST, McLendon RE, Batt D, Ramsey T *et al*. (2006). AAL881, a novel small molecule inhibitor of RAF and vascular endothelial growth factor receptor activities, blocks the growth of malignant glioma. Cancer Res 66: 8722–8730.

Shibuya M (2006). Vascular endothelial growth factor (VEGF)-receptor2: its biological functions, major signaling pathway, and specific ligand VEGF-E. Endothelium-J Endothelial Cell Res 13: 63–69.

Sridhar SS, Hedley D, Siu LL (2005). Raf kinase as a target for anticancer therapeutics. Mol Cancer Ther 4: 677–685.

Strowski MZ, Cramer T, Schafer G, Juttner S, Walduck A, Schipani E *et al*. (2003). Helicobacter pylori stimulates host vascular endothelial growth factor-A (vegf-A) gene expression via MEK/ERK-dependent activation of Sp1 and Sp3. FASEB J 17: 218–220.

Suzuki Y, Montagne K, Nishihara A, Watabe T, Miyazono K (2008). BMPs promote proliferation and migration of endothelial cells via stimulation of VEGF-A/VEGFR2 and angiopoietin-1/Tie2 signalling. J Biochem 143: 199–206.

Takahashi T, Ueno H, Shibuya M (1999). VEGF activates protein kinase C-dependent, but Ras-independent Raf-MEK-MAP kinase pathway for DNA synthesis in primary endothelial cells. Oncogene 18: 2221–2230.

Thompson N, Lyons J (2005). Recent progress in targeting the Raf/MEK/ERK pathway with inhibitors in cancer drug discovery. Curr Opinn Pharmacol 5: 350–356.

Turner A, Zsebo K, Martin F, Jacobsen F, Bennett L, Broudy V (1992). Nonhematopoietic tumor cell lines express stem cell factor and display c-kit receptors. Blood 80: 374–381.

Uchida T, Gao JP, Wang C, Satoh T, Itoh I, Muramoto M *et al*. (2001). Antitumor effect of Bcl-2 antisense phosphorothioate oligodeoxynucleotides on human renal-cell carcinoma cells in vitro and in mice. Mol Urol 5: 71–78.

Wang Z, Meng NN, Huang TT, Zhang YK, Yu LT (2010). 2-Methylcarbamoyl-4-{4-[3-(trifluoro-methyl)benzamido]phenoxy} pyridinium 4-methylbenzenesulfonate monohydrate. Acta Cryst E66: 1600–5368.

Wedge SR, Ogilvie DJ, Dukes M, Kendrew J, Chester R, Jackson JA *et al*. (2002). ZD6474 inhibits vascular endothelial growth factor signaling, angiogenesis, and tumor growth following oral administration. Cancer Res 62: 4645–4655.

Wilhelm SM, Carter C, Tang LY, Wilkie D, McNabola A, Rong H *et al*. (2004). BAY 43-9006 exhibits broad spectrum oral antitumor activity and targets the RAF/MEK/ERK pathway and receptor tyrosine kinases involved in tumor progression and angiogenesis. Cancer Res 64: 7099–7109.

Wu ZQ, Guo QL, You QD, Zhao L, Gu HY (2004). Gambogic acid inhibits proliferation of human lung carcinoma SPC-A1 cells in vivo and in vitro and represses telomerase activity and telomerase reverse transcriptase mRNA expression in the cells. Biol Pharm Bull 27: 1769–1774.

Xu Y, Zheng R, Zhou Y, Peng F, Lin H, Bu Q *et al*. (2011). Small molecular anticancer agent SKLB703 induces apoptosis in human hepatocellular carcinoma cells via the mitochondrial apoptotic pathway *in vitro* and inhibits tumor growth *in vivo*. Cancer Lett 313: 45–53.

Yi T, Yi Z, Cho SG, Luo J, Pandey MK, Aggarwal BB *et al*. (2008). Gambogic acid inhibits angiogenesis and prostate tumor growth by suppressing vascular endothelial growth factor receptor 2 signaling. Cancer Res 68: 1843–1850.

Zachary I, Gliki G (2001). Signaling transduction mechanisms mediating biological actions of the vascular endothelial growth factor family. Cardiovasc Res 49: 568–581.

Zhang Q, Feng W, Zhou HY, Yan B (2009). Advances in preclinical small molecules for the treatment of NSCLC. Expert Opin Ther Pat 19: 731–751.

Zou HY, Li QH, Lee JH, Arango ME, McDonnell SR, Yamazaki S *et al*. (2007). An orally available small-molecule inhibitor of c-met, PF-2341066, exhibits cytoreductive antitumor efficacy through antiproliferative and antiangiogenic mechanisms. Cancer Res 67: 4408–4417.

Supporting information

Additional Supporting Information may be found in the online version of this article at the publisher's web-site:

Figure S1 SPC-A1, A549, A375, HCT-116 and OS-RC-2 tumor-bearing athymic mice were treated with YL529 and body weights were determined. No changes in body weights were detected over the course of the experiment (n = 8).
Table S1 The hematological parameters of YL529 were determined after oral administration with a single dose an acute toxicity test in rats (n = 10). SPSS (SPSS, IL) software was used for statistical analysis ($P < 0.05$).
Table S2 The serum biochemistry parameters of YL529 were determined after oral administration with a single dose an acute toxicity test in rats (n = 10). SPSS (SPSS, IL) software was used for statistical analysis ($P < 0.05$).